Soft Matter

Accepted Manuscript

ROYAL SOCIETY OF CHEMISTRY

www.rsc.org/softmatter

ARTICLE TYPE www. rsc.org/xxxxxx | XXXXXXXX

Bond breaking dynamics in semiflexible networks under load

Christian Vaca,*[a] Roie Shlomovitz,[b] Yali Yang,[c] Megan T. Valentine,[c], and Alex J. Levine[a,d,e]

Received Xth XXXXXXX 20XX, Accepted Xth XXXXXXXXX 20XX
First published on the web Xth XXXXXXXXXX 200X
DOI: 10.1039/b000000x

Abstract

We examine the bond-breaking dynamics of transiently cross-linked semiflexible networks using a single filament model in which that filament is peeled from an array of cross-linkers. We examine the effect of quenched disorder in the placement of the linkers along the filament and the effect of stochastic bond-breaking (assuming Bell model unbinding kinetics) on the dynamics of filament cross-linker dissociation and the statistics of ripping events. We find that bond forces decay exponentially away from the point of loading and that bond breaking proceeds sequentially down the linker array from the point of loading in a series of stochastic ripping events. We compare these theoretical predictions to the observed trajectories of large beads in a cross-linked microtubule network and identify the observed jumps of the bead with the linker rupture events predicted by the single filament model.

1 Introduction

Semiflexible networks are materials composed of stiff filaments cross-linked densely on the scale of their own thermal persistence length. As such, the constituent filaments can support stress via bending as well as stretching. The study of such semiflexible gels has been inspired by their importance in cellular mechanics, where the semiflexible network of the cytoskeleton confers mechanical rigidity and is the source of force generation in eukaryotic cells. These studies have yielded a rich phenomenology including nonaffine deformation [1–3], continuous, zero-temperature phase transitions [4–6], complex nonlinear elasticity [7–10], and the active mechanics of motor-driven networks [11–16].

Understanding the collective mechanical response of such networks has implications for the dynamics [17] and mechanobiology of cells [18–20], but also offers new insights into fundamental mechanical properties of this special class of polymer gels – fiber networks rather than flexible (Gaussian coil) polymer gels. One feature of these networks receiving renewed attention is the role of cross-linker mechanics in the collective response of the network. These include exploring the mechanical effect of flexible cross-linkers [21,22], cross-linker protein domain unfolding [23,24], and cross-linker unbinding [8,25,26]. The latter effect is particularly interesting as this allows for structural rearrangements on long time scales either as the network approaches thermal equilibrium [27] or in the response to applied loads [28,29].

Our previous experiments [28] on the motion of a bead (with a radius much larger than the mesh size of the network) show that there is a regime of creep in which the bead moves with constant velocity v in response to a constant applied force F. Energy dissipation in the network results primarily from bond breaking as can be inferred from the observed force-velocity relation, $\log(v) \sim F$, consistent with a Bell model for ligand unbinding rates [30]. In spite of this bond breaking, the modulus of the network remains essentially unchanged. One infers that bond breaking and reformation occur at equal rates in the loaded network. Closer examination of the beads' trajectories reveals many small stochastic hops on the scale of tens of nanometers, suggesting that one can indeed resolve individual bond breaking events within the large-scale drift of the bead under load.

In this article we explore a single filament model for such bond breaking events, which we use to understand a few fundamental features of the dissipative dynamics in the constant velocity regime. In order to apply our results to cross-linked microtubule networks, which is the system of experimental interest, we ignore entropic effects. This very stiff network is effectively a zero temperature system; as such our analysis should apply equally well to a variety of fiber networks and fiber-reenforced composites. We examine the spatial distribution of mechanical loading of the many non-covalent cross-linking bonds between filaments and develop a statistical model for the bond breaking dynamics. Using this model we reexamine the apparently uniform motion of the bead, which can be resolved into a series of microscale jumps, and conclude that these dynamics are consistent with the bond-breaking of just the highly loaded cross-linkers in the immediate vicinity of the bead. This bond breaking is consistent with a picture of bond breaking occurring on many different

[a] *Department of Physics & Astronomy, UCLA, Los Angeles, CA 90005.*
[*] *Corresponding Author*
[b] *Mediguide Ltd, St. Jude Medical, Haifa, Israel.*
[c] *Department of Mechanical Engineering, UCSB, Santa Barbara, CA 93106.*
[d] *Department of Chemistry & Biochemistry, UCLA, Los Angeles, CA 90005.*
[e] *Department of Biomathematics, UCLA, Los Angeles, CA 90005.*

filaments rather than sequential breaking of bonds along a single filament. The network remodels with many independent events occurring on many filaments rather than in the peeling away of any one filament in particular. We conclude with a discussion of further experimental tests of this emerging understanding of the network's failure and a few speculations on the appearance of cross-linker unbinding deformation in such transiently cross-linked fiber networks.

2 Single Filament Model

We begin with a single filament model. As shown in Fig. 1a, the filament in question (shown as a dashed line) is being deflected by the bead (large sphere); it is also bound to the network (solid lines) by a random set of cross-linkers (small spheres). In our single filament analysis we replace the entire network by an array of posts along the $\hat{z}$ axis to which the single filament is bound – see Fig. 1*b*. The bead is replaced by point loading at the origin of the coordinate system. Here we control either the load or the displacement. If the bead filament interaction allows for slip, it may generate only perpendicular forces; sticky beads may also apply longitudinal forces along the filament leading to tension. We consider both cases below, but begin with the more simple case of slip boundary conditions and perpendicular loading of the filament.

We assume that bond breaking, when it occurs, is instantaneous and that the time between bond breaking events is long compared to the relaxation time of filaments, so that filament evolves from one static mechanical equilibrium configuration to the next upon each bond breaking event. This separation of time scales is explored more fully in appendix A. To understand the loading of these bonds in static equilibrium, we must first determine the forces on the cross-linkers for a semiflexible filament linked to a spatially random set of cross-linkers.

Taking the undeformed state of the single filament to be straight and $\zeta(z)$ to be the perpendicular displacement of the filament in response to the applied force F acting at the origin, we write the elastic free energy $\mathscr{F}$ of the filament under uniform tension τ as[31]

$$\mathscr{F} = \int_{L_c} dz \left[\frac{\kappa}{2} \left(\partial_z^2 \zeta(z)\right)^2 + \frac{\tau}{2} \left(\partial_z \zeta(z)\right)^2 + \right. \\ \left. + \frac{V(z)}{2} \left(\zeta(z)\right)^2 - F\,\delta(z)\,\zeta(z) \right]. \qquad (1)$$

Here κ is the bending rigidity of the filament, which is related to the filament's elastic moduli and cross sectional geometry in the usual way[31]. The function $V(z)$ represents the harmonic interaction of filament with the cross-linkers and the rest of the network. We take this to be

$$V(z) = K \sum_i \delta(z - z_i), \qquad (2)$$

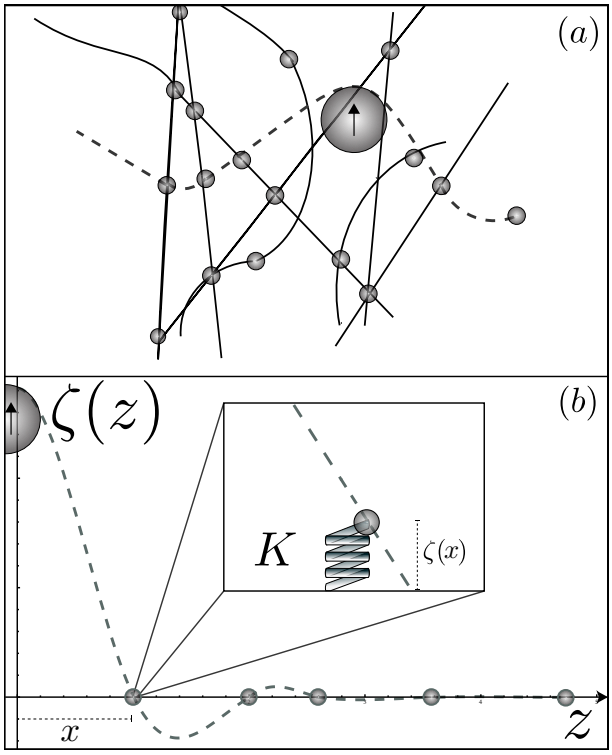

Fig. 1 (*a*) A single filament of interest (dashed line) embedded in a cross-linked filament network (solid lines) being deformed by a force F transmitted by the probe particle (large shaded circle). (*b*) The deflection $\zeta(z)$ of that same filament in a two-dimensional, single filament model, where the undeformed (straight) filament is bound to a random array of cross-linkers along the $\hat{z}$-axis. x is the position of the nearest cross-linker to the applied force.

where the set of linker locations $\{z_i | i = 1,\ldots,N\}$ are quenched stochastic variables chosen so that there is a Poisson distribution of lengths between adjacent linkers – see Ref.[1] for details – with mean length $\bar{\ell}$ between consecutive cross-linkers. The elastic compliance K^{-1} of the linkers is meant to reflect the combined compliance of the linking molecules and the filament network in which they are embedded. The latter compliance dominates the former so that $K \sim 6\pi G_0 a$, where G_0 is the plateau modulus of the network and a a size characteristic of the bond to network connection. Taking $a \sim 10^{-9}$m and gel moduli in the kPa or softer range, we find $K \sim 10^2$pN/μm.

Minimization of Eq. 1 with respect to the deflection field yields the condition for force balance obeyed by the filament in between bond breaking events

$$\kappa\,\partial_z^4 \zeta(z) - \tau\,\partial_z^2 \zeta(z) + V(z)\zeta(z) = F\,\delta(z). \qquad (3)$$

From this equation and the mean length between consecutive cross-linkers, one obtains two fundamental length scales – the

potential length ℓ_p and the bending length ℓ_κ defined respectively to be

$$\ell_p = \left(\frac{144\,\kappa\bar{\ell}}{K}\right)^{1/4}; \quad \ell_\kappa = \left(\frac{\kappa}{\tau}\right)^{1/2}. \tag{4}$$

The potential length is a measure of how far the deflection field of the filament due to the applied point force penetrates past the first unbroken cross-linker. As one might expect, this penetration depth grows with the elastic compliance of linkers K^{-1} and with the bending modulus of the filament*.

The bending length measures the relative importance of bending and tension in the force balance relation. Forces associated with filament bending are related to higher derivatives of the filament configuration, and thus always dominate at sufficiently short distances. At distances greater than the bending length ℓ_κ, tension rather than bending plays the dominant role in the force balance relation, Eq. 3. At those length scales, the mechanics of the filament is more analogous to that of a taut string. We will see that for distances small compared to the bending length ℓ_κ the stiff filament acts like a lever, leading to an acceleration of the rate of subsequent unbinding events, as described in Section 2.2-see Fig. 4 inset.

Our analysis proceeds as follows. First we calculate all of the forces on the cross-linkers by solving Eq. 3 for states of mechanical equilibrium either with prescribed displacement or force at the origin. Using the calculated forces on the cross-linkers, we calculate the dissociation rates of the cross-linkers. We note that, due to the exponential dependence of the linker unbinding rate on force and the exponential decrease of the loading on the cross-linker with distance from the point of force application, it reasonable to assume that linkers break in sequence – the surviving linker currently nearest the point of force application is overwhelming most likely to break next. Using this observation, we make the *sequential unbinding approximation* and then compute the dynamics of filament unbinding. We then turn to the experiments. For the reader's convenience we provide a complete list of variables used in Table 1.

2.1 States of mechanical equilibrium

The solution of the mechanical equilibrium of the filament is facilitated by a transfer matrix approach. In the intervals of length $\ell_{i+1} = z_{i+1} - z_i$ between consecutive cross-linkers, we solve Eq. 3 with a shifted independent variable:

$$y_i = z - z_i, \tag{5}$$

* The numerical prefactor 144 is included to simplify later calculations.

where we define $z_0 = 0$. In this way the deflection field $\zeta_i(y_i)$ between the i^{th} and $(i+1)^{\text{th}}$ linker is simply given by

$$\begin{aligned}\zeta_i(z) =& \zeta_i^{(0)} + \zeta_i^{(1)} y_i + \zeta_i^{(2)} \ell_\kappa^2 \left[\cosh\frac{y_i}{\ell_\kappa} - 1\right] \\ &+ \zeta_i^{(3)} \ell_\kappa^3 \left[\sinh\frac{y_i}{\ell_\kappa} - \frac{y_i}{\ell_\kappa}\right],\end{aligned} \tag{6}$$

in terms of the (as yet unknown) boundary conditions: $\zeta_i^{(n)}$, $n = 0, \ldots, 3$ representing the displacement $\zeta_i^{(0)}$ at the i^{th} linker and its first three derivatives. In the limit of no tension, Eq. 6 becomes

$$\zeta_i(z) = \zeta_i^{(0)} + \zeta_i^{(1)} y_i + \zeta_i^{(2)} \frac{y_i^2}{2!} + \zeta_i^{(3)} \frac{y_i^3}{3!}, \tag{7}$$

as is clear from taking the appropriate limit of Eq. 6. In both cases, the solution is written in terms of the four unknown parameters.

Since the filament must be continuous and have continuous first and second derivatives, knowing the solution for the filament in the i^{th} segment $\ell_i = z_i - z_{i-1}$ provides these three boundary conditions for the solution of the filament trajectory in the next segment $\ell_{i+1} = z_{i+1} - z_i$. Integration of Eq. 3 across z_i yields the discontinuity in $\zeta'''(z)$, which is determined by the harmonic force provided by that linker: $\zeta_i'''(0) - \zeta_{i-1}'''(\ell_i) = -\frac{K}{\kappa}\,\zeta_{i-1}(\ell_i)$.

Imposing these boundary conditions across the i^{th} cross-linker amounts to solving a linear system of equations for $\zeta_{i+1}^{(n)}$ in terms of the analogous information at the previous cross-linker $\zeta_i^{(n)}$. Thus, the effect of the solution of the differential equation for the filament trajectory between cross-linkers is to propagate that boundary condition information forward via a linear transformation, which may be described in terms of a transfer matrix

$$\zeta_{i+1} = T(\ell_i)\,\zeta_i, \tag{8}$$

where $\zeta_i = \{\zeta_i^{(0)}, \zeta_i^{(1)}, \zeta_i^{(2)}, \zeta_i^{(3)}\}$. The full transfer matrix is readily computed from the solutions given in Eqs. 6,7 for the cases of finite and zero tension respectively. The matrix is shown in Appendix C.

Iteration of the transfer matrix on the vector representing the state of the filament at the point of force application yields the state of the filament at an arbitrary cross-linker: ζ_n: $\zeta_n = [T(\ell_n)T(\ell_{n-1})\ldots T(\ell_1)]\,\zeta_0$. The differential equation solutions then give the correct form of the filament's trajectory in force balance in between these site. However, since our interest is solely in the forces at the linkers, the full filament trajectory information is unnecessary.

It remains to determine the initial boundary condition vector ζ_0 at the site of force application. We choose to apply a point force F and we require a zero tangent condition: $\zeta_0^{(1)} = 0$,

Table 1 List of variables. Dimensions: $[L]$ =Length, $[t]$ =time, and $[F]$ =Force.

Symbol	Dimensions	Description
z	$[L]$	Position along contour length of undeformed filament
z_i	$[L]$	Position of i^{th} cross-linker down filament's undeformed contour length, L_c
$\ell_i = z_i - z_{i-1}$	$[L]$	Distance between i^{th} and $(i-1)^{\text{th}}$ cross-linker
x	$[L]$	Distance to nearest unbroken cross-linker from applied force, F
$\zeta(z)$	$[L]$	Deflection field of filament perpendicular to undeformed configuration
ζ_i	$\{[L],1,[L]^{-1},[L]^{-2}\}$	Vector of derivatives of the deflection field at i^{th} cross-linker
κ	$[F][L]^2$	Bending modulus of filament
τ	$[F]$	Applied tension on filament
K^{-1}	$[L]\ [F]^{-1}$	Elastic compliance of cross-linkers
ℓ_p	$[L]$	Potential length
ℓ_κ	$[L]$	Bending length
$\bar{\ell}$	$[L]$	Mean distance between cross-linkers
F	$[F]$	Applied force
$T(\ell_i)$	Multiple dimensions	Transfer matrix (see appendix C for dimensions of elements)
k	$[t]^{-1}$	Bell model dissociation rate (base rate of cross-linker dissociation)
k_0	$[t]^{-1}$	Base rate of cross-linker dissociation
F_0	$[F]$	Thermal force scale
$\mathscr{T}$	$[t]$	Total time of dissociation of a filament from cross-linker density
$P_m(t)$	1	Probability that m cross-linkers have dissociated by time t
$v_\perp(x)$	$[L]\ [t]^{-1}$	Normal velocity of point of loading for a cross-linker at x
$\mathscr{P}_N(n)$	1	Probability of n sequential peeling events occurring over one mean dissociation time τ on a filament bound to N cross-linkers

i.e, a "clamped" boundary condition. Of course, there are two other boundary conditions needed to determine the initial value of the vector ζ_0, as is expected for the fourth order differential equation Eq. 3. We must specify these at the other end of the filament. There are two classes of problems that one may address. For finite length filaments, we may require the far end to be both force and torque free. For infinite length filaments, we will assume that the filament and its local slope both approach zero: $\zeta_i^{(0,1)} \to 0$ for $i \to \infty$. Both cases are discussed further below.

2.2 An infinite filament interacting with a lattice of linking sites

The simplest solution is obtained for the case of an infinite filament with an ordered lattice of binding sites. In this case $\bar{\ell} = z_{i+1} - z_i$ for all i and the product of transfer matrices necessary for the solution becomes simply the n^{th} power of one transfer matrix. This problem is best addressed by working in the eigenbasis of the transfer matrix. There are four complex eigenvalues λ_i, which are the roots of the polynomial

$$\lambda_i^4 + 1 - (\lambda_i^3 + \lambda_i)(2 + 2\cosh\gamma + 144\,\frac{\alpha}{\gamma^2} - 144\,\frac{\alpha}{\gamma^3}\sinh\gamma)$$
$$+2\lambda_i^2(1 + 2\cosh\gamma + 144\,\frac{\alpha}{\gamma^2}\cosh\gamma - 144\,\frac{\alpha}{\gamma^3}\sinh\gamma) = 0.$$

These roots are functions of two dimensionless control parameters: $\alpha = \left(\bar{\ell}/\ell_p\right)^4$ and $\gamma = \bar{\ell}/\ell_\kappa$. The first measures the (fixed) distance between binding sites in terms of the potential length. The second compares the same inter-binding site distance to the bending length.

In Fig. 2a we plot the logarithm of the modulus of these four eigenvalues $\lambda_i = \lambda_i(\alpha,\gamma)$ as a function of α for fixed $\gamma = 5$. This plot shows a number of generic features that characterize all solutions. Two of the four eigenvalues have a modulus greater than one and two less than one; this point will be essential when studying the infinite filament solutions below. For any nonzero value of γ (i.e., for finite tension in the filament) there are three classes of roots $\lambda_i = \lambda_i(\alpha,\gamma)$. For sufficiently small α, one finds the *high tension regime* where there are four distinct real eigenvalues, shown in the figure as dashed lines. The subspace spanned by the eigenvectors with eigenvalues having magnitudes less than one span the set of all monotonically decaying displacement field solutions. In this limit where the tension is high and the linker compliance is also large, the relaxation of the filament back to the axis containing the linkers is generically a double exponential decay. A typical solution is shown by the dashed line in Fig. 2b.

For larger α, one encounters the *incommensurate regime* where the eigenvalues come in two complex conjugate pairs. These four solutions are represented by the solid lines in Fig. 2a (the complex conjugate pairs necessarily have the same modulus). The subspace spanned by the decaying solutions

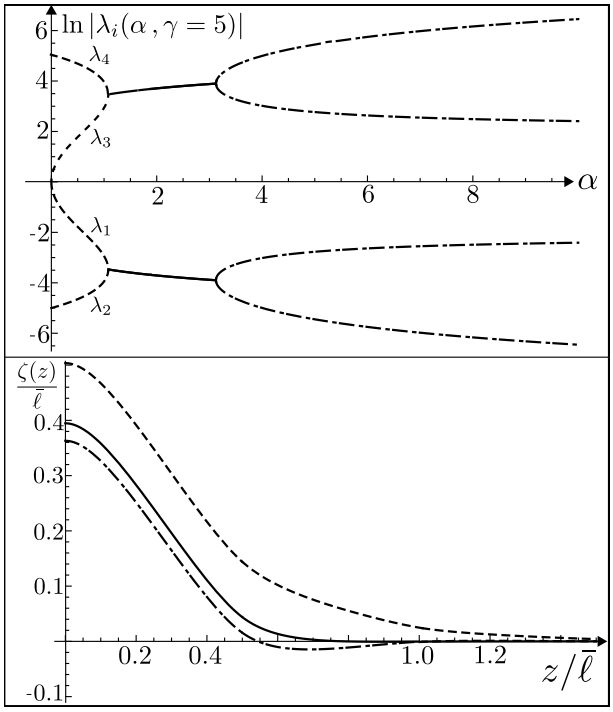

Fig. 2 (Top) The log of the modulus of the four eigenvalues as a function for α for a tensed filament: $\gamma = 5$ showing the high tension, incommensurate, and lock-in regimes, as described in the text. (Bottom) Typical filament deflections for a filament of infinite length interacting with a a lattice of linker sites in the high tension (dashed), incommensurate (solid) and lock-in (dash-dotted) regimes.

(corresponding to eigenvalues with modulus less than unity) takes the form $\zeta_n \sim \exp(-kn)\cos(n\phi)$. The filament's displacement decays exponentially but overshoots the linkers positions. Since the phase angle ϕ is generically not a rational fraction of 2π, the periodicity of the height field at the linkers is typically incommensurate with the linker lattice – a solution of this type is shown by the solid line in Fig. 2b. For even larger α corresponding to more incompliant linkers, these incommensurate undulations lock-in with the lattice leading to a form $\zeta_n \sim \exp(-kn)\cos(n\pi)$. A typical solution of this form is shown by the dash-dotted line in Fig. 2b. For zero tension, the transition from incommensurate to commensurate filament undulations remains, but the high tension region vanishes.

We first consider the case of infinitely long filaments. Finite length effects are addressed in the next section. The known applied force at the origin and the clamped (zero slope) boundary condition determine two of the four unknown coefficients $\zeta_0 = \left\{\zeta_0^{(0)}, 0, \zeta_0^{(2)}, -F/\kappa\right\}$. To solve the filament trajectory and, from that, the loading on each of the linkers for an infinite filament one must work in the subspace spanned by the eigenvectors $\mathbf{w}_{1,2}$ corresponding to the small modulus ($|\lambda_{1,2}| < 1$) eigenvalues in order to obtain decaying solutions. We expand the solution in terms of two unknown coefficients $\zeta_0 = b_1\mathbf{w}_1 + b_2\mathbf{w}_2$. These are given by

$$b_1 = \frac{F}{\kappa}\frac{(\lambda_1-1)(\lambda_2+1)(\lambda_1-\cosh\gamma)}{(\lambda_1-\lambda_2)(\lambda_1\lambda_2+\lambda_1+\lambda_2-2\cosh\gamma-1)}$$

$$b_2 = \frac{F}{\kappa}\frac{(\lambda_2-1)(\lambda_1+1)(\lambda_2-\cosh\gamma)}{(\lambda_2-\lambda_1)(\lambda_1\lambda_2+\lambda_1+\lambda_2-2\cosh\gamma-1)}.$$

Recalling that each linker is a Hookean spring, it is simple to obtain the force on each linker: the force on the i^{th} linker F_i is simply linear in the deflection at that point and proportional to the spring constant

$$F_i = K\left(b_1\,\lambda_1^i\,w_1^0 + b_2\,\lambda_2^i\,w_2^0\right) \tag{9}$$

where w_i^0 is the first component of the i^{th} eigenvector corresponding to $\zeta^{(0)}$, the deflection field.

In order to follow the dynamics of bond breaking, one needs to know how these forces are redistributed after each linker dissociation event. Anticipating the sequential breaking assumption (to be justified by the exponential decay of forces along the filament) we focus on the case in which the first p cross-linkers have failed. To take into account the load redistribution after p cross-linkers have been dissociated, we replace the first $(p+1)$ transfer matrices in the product by one with an increased inter-linker distance. The solution for the filament trajectory at the surviving linker sites $n > p+1$ is then given by ζ_n with

$$\zeta_n = T\left[\bar{\ell}\right]^{n-(p+1)} T\left[(p+1)\,\bar{\ell}\right]\,\zeta_0. \tag{10}$$

The analysis now proceeds along the same lines, but the state vector of the filament after the first unbroken cross-linker must remain in the subspace spanned by the two decaying modes. Thus, the boundary conditions at the point of force application are chosen to give $T\left[(p+1)\,\bar{\ell}\right]\,\zeta_0 = b_1\mathbf{w}_1 + b_2\mathbf{w}_2$.

We show in Fig. 3 the absolute value of the deflection field for an infinite semiflexible filament interacting with a lattice linker sites before any bond dissociations. Parameters are chosen so that the filament is in the locked-in regime – see Fig. 2b. The semilog plot demonstrates the exponential decay of the envelope of oscillations the deflection amplitude (dotted line). As consequence, the cross-linker loading is largest on the first unbroken linker. In fact, for a total force F, the load on the first linker is typically greater than the applied force $\sim 2F$. This and Bell model for cross-linker disassociation rates justifies our sequential unbinding approximation for the dynamics – see Sec. 3.

Given the sequential breaking assumption, one must determine the load on the first unbroken linker after the first p linkers have already been broken. This is straightforward using

Eq. 10 and the harmonic linker potential to convert the deflection to a force. We plot the result in Fig. 4. For $\tau = 0$, there is a linear increase in the force due to a lever arm effect[32,33].

The array of unbroken cross-linkers provides the fulcrum

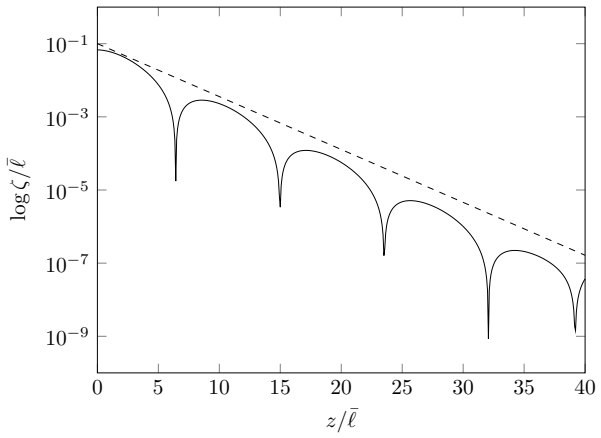

Fig. 3 Absolute value of the deflection of an infinite semiflexible filament interacting with a lattice of binding sites in the locked-in regime showing oscillations and an exponential envelope (dashed line).

of the lever, and the lever arm is the section of the filament that has already undergone cross-linker dissociation – see inset. Subsequent breaking events increase the lever arm and the mechanical advantage of the load, suggesting that peeling dynamics should accelerate. Finite tension $\tau > 0$ cuts off this growth at $\sim \ell_\kappa$. More details on the effect of finite tension on the configuration of and force distribution on the filament are discussed in appendix B.

2.3 Finite length corrections

We now examine the forces on the finite contour length filament for an ordered array of cross-linkers. We take the end of the filament to be force and torque free, setting $\zeta_N = \{\zeta_N^{(0)}, \zeta_N^{(1)}, 0, 0\}$ at the end of the filament so that there are two boundary conditions to be satisfied on each end of the filament. We recapitulate the transfer matrix solution for the finite filament with p broken linkers using Eq. 10 and solving for the four unknown constants, $x = \{\zeta_0^{(0)}, \zeta_0^{(2)}, \zeta_N^{(0)}, \zeta_N^{(1)}\}$. Solving this linear system of equations can be done as follows. Writing the matrix $M = T^{N-(p+1)}\left[\bar{\ell}\right] T\left[(p+1)\bar{\ell}\right]$ in terms of the column vectors $(\vec{m}_1, \vec{m}_2, \vec{m}_3, \vec{m}_4)$, and introducing unit column vectors in the 1 and 2 directions, $\hat{e}_{1,2}$ respectively, one may write linear system of equations in the form

$$\zeta_0^{(0)}\vec{m}_1 + \zeta_0^{(2)}\vec{m}_3 - \zeta_N^{(0)}\hat{e}_1 - \zeta_N^{(1)}\hat{e}_2 = -\frac{F}{\kappa}\vec{m}_4, \qquad (11)$$

which may be inverted to obtain the four undetermined coefficients. To briefly summarize, we find that for ordered arrays

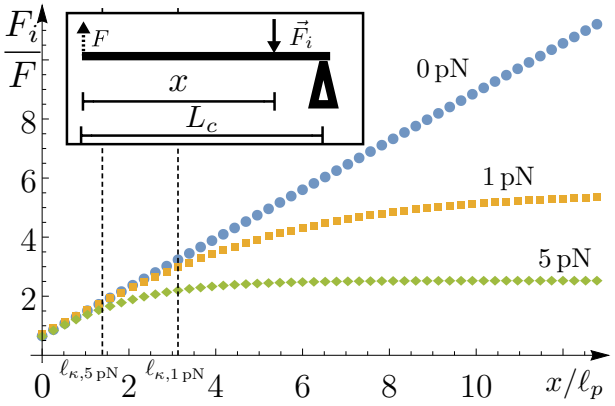

Fig. 4 Force on the first unbroken cross-linker after i cross-linkers have already broken in the linker lattice at various tensions. The lever arm effect provides increasing mechanical advantage for subsequent linker peeling over distances ℓ_κ. x is the distance to the nearest cross-linker to the applied force, F. Lengths measured in units of ℓ_p Inset: Diagram of the "class two" lever where the load (cross-linker force, F_i) lies between the effort (applied force, F) and the fulcrum (the remaining cross-linkers not undergoing dissociation).

of linkers, the effect of finite length becomes significant only in a region of length $\sim \ell_p$ near the ends, assuming that the filament is at least of order ℓ_p. For disordered arrays of the linkers, it appears that the infinite length filament approximation also remains valid for some region at least a few ℓ_p away from the ends.

2.4 Random arrays of linkers

In a random isotropic network, one expects that the distribution of distances between consecutive cross-linkers to be random with a Poisson distribution. Specifically, given a mean distance $\bar{\ell}$ between cross-linkers, the probability of finding a distance between consecutive linkers between z and $z+dz$ is $P(z)dz = \exp\left[-z/\bar{\ell}\right]/\bar{\ell}\, dz$. This implies that there will be exponentially rare long gaps, i.e., much larger than the mean spacing, between cross-linkers. Understanding the effect of such quenched random linker positions on the unpeeling process is important for assessing the implications of the simple lattice model for more physical random filament networks.

To explore this issue, we generated an ensemble randomly pinned filaments using products of transfer matrices $\Pi_{i=1}^{N} T(\ell_i)$, with the distance between the cross-linkers, ℓ_i, selected from a Poisson distribution in place of the simple product of identical transfer matrices used in Eq. 10. For all simulations discussed below, the following values of material parameters of the semiflexible filament were used: (when applicable) $\tau = 5\,\mathrm{pN}$ and $K = 100\,\mathrm{pN}/\mu\mathrm{m}$. The results are summarized in Fig. 5, where we see that the distribution of load-

ing on the first unbroken cross-linker in the disordered case (solid line) lies mostly to the left of that force for the linker lattice having the same mean spacing as the disordered array. The preponderance of these lower forces leads to generically slower peeling dynamics in disordered linker arrays as compared to regular ones at the same mean linker density. We directly observe this effect in the calculation of the dynamics – see Fig. 7.

3 Peeling dynamics

Having examined the problem of mechanical equilibrium, we turn to the question of forced peeling dynamics of a single filament from an array of linkers. The disassociation of non-covalent bonds are generally well-understood in terms of the Bell model[30], which postulates that the unbinding rate k is exponentially sensitive to force applied to that bond

$$k(F) = k_0 e^{F/F_0}, \tag{12}$$

where both the zero force off-rate and the force scale F_0 depend on microscopic parameters specific to the linker in question. For biotin avidin bonds the force scale is $F_0 \sim 30$ pN[28] Subsequently, much work has been done on the effect of the loading rate on the mean force[34] of rupture in force-ramp experiments. We expect that loading to be rapid compared to the mean time to failure for a bond, and neglect the dependence

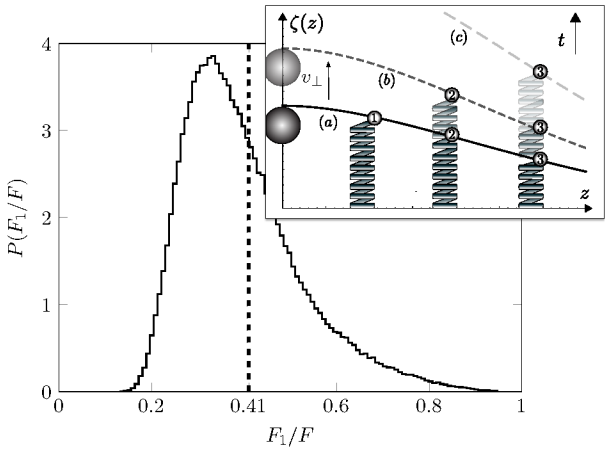

Fig. 5 Distribution of loading on the first unbroken linker for Poisson distributed cross-linkers on a single filament. The equivalent loading for a regular linker array with the same inter-linker mean spacing is shown as the dashed line. Inset: Schematic of sequential peeling showing filament after zero (a), one (b), and two (c) linker rupture events.

on loading rate. The stochastic nature of the unbinding process implies that, although the linker loading is deterministic, the peeling dynamics are always stochastic. It is essential to distinguish between the two different types of random variables in this problem: the stochastic dynamics associated with the unbinding of a given linker and the quenched random distribution of linker positions along a filament.

Based on the exponential dependence of the unbinding rate upon load – see Eq. 12 – and exponential decay of the bond loading on subsequent linkers moving down the filament from the point of loading – see Fig. 3 – the first unbroken linker is always significantly more likely to break than any of the others. Based on this, we introduce the sequential unbinding approximation in which we consider a special (but more significantly probable – see appendix D) sequence of breaking events in which only first unbroken linker fails. This limits our analysis to a particular subclass of stochastic trajectories of the filament under loading and greatly simplifies the analysis. A schematic of the allowed unpeeling trajectories is shown in in the inset of Fig. 5 in which we define $v_\perp$, the velocity of the point of loading normal to the initial direction of the undeformed filament.

Given the force-dependent bond rupture rate, it is a simple matter to write the bond survival probability[35,36] at time t after having been loaded with force F at $t = 0$: $p(t) = \exp[-k(F)t]$. To study the stochastic dynamics of the unpeeling process, we need to calculate the probability that the m^{th} cross-linker breaks in an infinitesimal interval of time dt at time t after initially loading the filament at the origin.

To determine this we must integrate over all allowed (i.e., sequential) breaking trajectories. In other words, each of the N bonds ruptures in turn, causing the filament to redistribute the load on the surviving bonds. From this series of stochastic events, one may define the survival probability of the m^{th} bond at a time t after the filament is initially loaded at the ori-

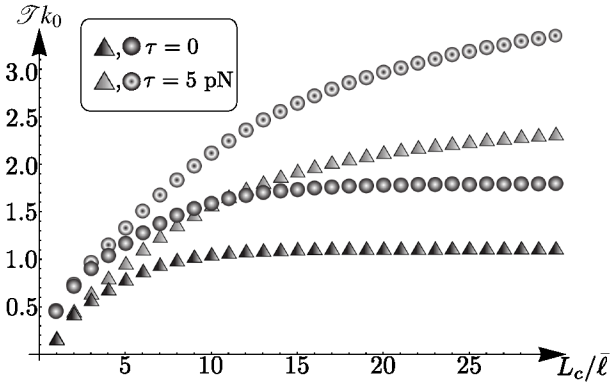

Fig. 6 $\mathscr{T}$ as a function of filament length L_c for a regular lattice (triangles) and Poisson distribution (circle) of cross-linkers-see Eqn 17. Distances are measured in mean linker spacings $\bar{\ell}$. In the tensionless cases (filled symbols) the lever-arm effect accelerates peeling. In all cases, disorder slows the mean peeling rate, due to "trapping regions" having anomalously high linker density.

gin, $P_m(t)$. This may be written as a integral over all intervals of time t_k between the rupture of bonds $k-1$ and k for the first $k = 1,\ldots m-1$ bonds. These bonds must break before the m^{th} bond, which is next to break (assuming sequential breaking). The sum of these intervals and time that the m^{th} bond has survived as the next to break must add to the total time t. The integral is given by

$$P_m(t) = \int_0^t dt_m \int_0^{t_m} dt_{m-1} \ldots \int_0^{t_2} dt_1 \exp[-k_1 t_1] k_1 \times \exp[-k_2(t_2 - t_1)] k_2 \ldots k_m \exp[-k_{m+1}(t - t_m)], \quad (13)$$

where the breaking rates $k_1,\ldots,k_{m+1}$ are determined by the solution of the mechanics problems previously discussed. The evaluation of those rates lies at the heart of the calculation.

Assuming those rates are known, the evaluation of the integral is straightforward:

$$P_m(t) = (-1)^m \left(\prod_{i=1}^{m} k_i\right) \left(\sum_{q=1}^{m+1} \frac{\exp[-k_q t]}{Y(q,m)}\right);$$

where

$$Y(q,m) = \prod_{j\neq q}^{j\leq m+1} (k_q - k_j). \quad (14)$$

Taking the time derivative of $P_m(t)$ in Eq. 13, one may obtain a recursive set of differential equations for the various bond-breaking probabilities. These have a simple interpretation, which is discussed in appendix E.

The probability for bond m to break is the negative derivative that bond's survival probability [36]

$$f_m(t) = -\frac{d}{dt}\left(\sum_{q=0}^{m} P_q(t)\right) = k_{m+1} P_m(t). \quad (15)$$

From this we compute the quantity of primary interest: the mean time for the rupture of the m^{th} linker along the filament. This mean τ_m, which is the first moment of the distribution $f_m(t)$ given by Eq. 15 is equal to the product of the m breaking rates of that bond and the earlier bonds

$$\tau_m = \int_0^\infty dt\, f_m(t)\, t = \sum_{q=1}^{m} \frac{1}{k_q}. \quad (16)$$

Setting $m = N$ and using Eq. 12, we obtain the total time for filament peeling

$$\mathscr{T} = k_0^{-1} \sum_{i=1}^{N} e^{-F_i/F_0}, \quad (17)$$

where F_i is the force on the first unbroken bond after bonds $1,\ldots,i-1$ have broken. The result is proportional to the fundamental rupture time scale $1/k_0$, specific to the linkers in question.

3.1 Asymptotic peeling rates for long filaments

From this linker-breaking scenario for the dissipative dynamics of the network, one must associate the loading time sufficient to cause plastic deformation with the time required for a typically filament to be peeled off of its original links to the network. Thus the mean time for rupturing a significant fraction of linkers from a very long filament gives a prediction of the model for the loading time required for plastic deformation as a function of applied force. Calculating the mean peeling time remains a complex problem for disordered linker arrays and even for ordered linker lattices since the loading on the i^{th} linker generically has a nontrivial dependence on linker number i.

For peeling a very long filament, however, the asymptotic peeling dynamics reached after many bond ruptures is more easily analyzed. Examining Fig. 4, we note that in the tension free case, the linker loading increases linearly with linker number: $F_i = \Xi\, i$ due to the lever arm effect. For the case of tensed filaments, the loading plateaus after a finite number of linker ruptures: $F_i = \Xi'$, independent of i. Using these approximations for all of the rupture events contributing to the mean peeling time, one may simply perform the sum in Eq. 17 to find for the tension-free case with accelerating peeling

$$\mathscr{T} k_0 = \frac{e^{-\Xi/F_0} - e^{-\Xi(N+1)/F_0}}{1 - e^{-\Xi/F_0}}. \quad (18)$$

Due to the unbounded acceleration of the peeling, an infinite number of linkers $N \to \infty$ may be broken in finite time. This unphysical outcome results from our neglect of inertia in the problem, but the high peeling velocity case is not of physical interest as larger displacements of the filament associated with the massive lever arm effect necessarily generate tension. Turning to the case with tension, leading to constant velocity peeling, we find the simple result

$$\mathscr{T} k_0 = N e^{-\Xi'/F_0}. \quad (19)$$

We tested these approximate solutions to the problem of average peeling dynamics for both ordered and disorder linker arrays using respectively analytic solutions and numerical simulations. In all cases, mean peeling time scaled with load F as predicted by the above results and the best fit was obtained using $\Xi'/F = 1.92$ and $\Xi/F = 0.25$ (using the values from Fig. 6). The first result demonstrates the force overshoot leading to a linker loading almost twice that of the applied force; the second shows that, without tension, the loading on

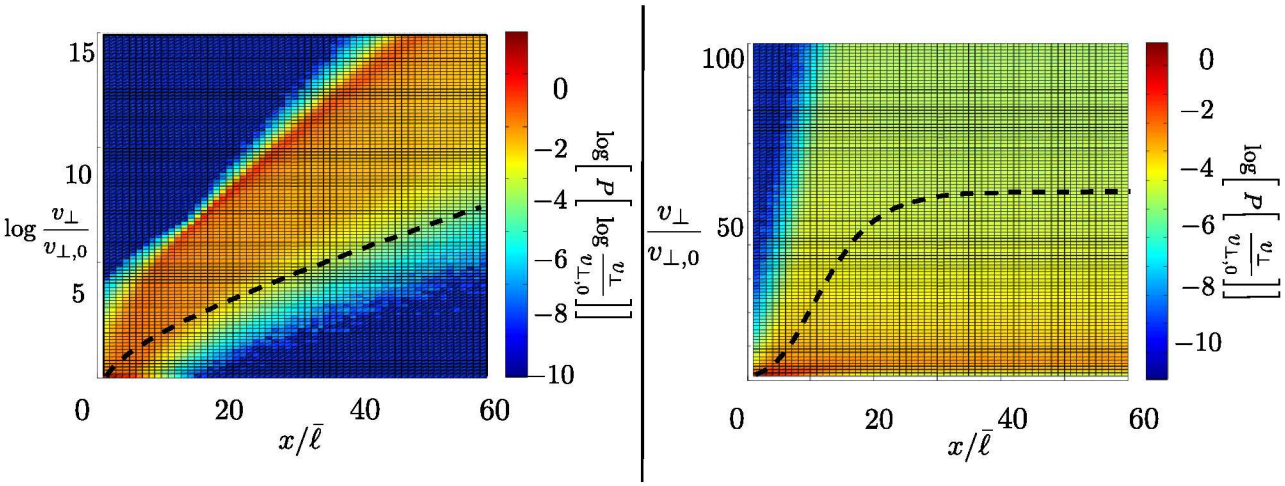

Fig. 7 (Left) Distribution of the logarithm of the perpendicular velocities with $\tau = 0$ showing the predicted peeling acceleration due to the lever arm effect holds in a random array of linkers. Dashed line corresponds to the velocity for an ordered array of cross-linkers. (Right) the same distribution for $\tau = 5\,\mathrm{pN}$, but on a linear scale (right). Here the peeling velocity approaches a constant as predicted based on the lattice calculations.

sucessive linkers during the peeling grows by one quarter of the total applied force. We now turn to the peeling dynamics simulations in disordered linker arrays.

3.2 Peeling dynamics in disordered linker arrays

To explore the single-filament peeling dynamics numerically, we constructed an ensemble of linker distributions for filaments in which the distance to the first linker is from 1 to 60 $\bar{\ell}$. Each filament had a total of 40 linkers, so 39 linkers were distributed beyond the first one. We consider both ordered linker arrays and disordered ones in which the interlinker spacing is selected from a Poisson distribution[1]. The stochastic peeling dynamics were simulated by computing the loading on the first unbroken linker and then selecting a waiting time for rupture using the Bell model. The results are plotted in Fig. 6. The spatial disorder increases the total time of peeling relative to the linker lattice when the mean linker separation in the disordered case is chosen to be equal to the lattice constant in the ordered one. For each simulated unpeeling event, we compute the normal velocity of the point of loading $v_\perp$,

$$\frac{v_\perp(x)}{v_0} = \frac{\Delta\zeta_0^{(0)}(x)\,k(x)}{\bar{\ell}\,k_0}, \qquad (20)$$

defined by the product of the jump in the normal displacement of the filament at the point of loading $\Delta\zeta_0^{(0)}$ upon a bond rupture at point x down the filament and the rate of bond breaking of that linker $k(x)$. This velocity is nondimensionalized by the product of the mean interlinker distance and the zero force bond breaking rate $\bar{\ell}k_0 = v_0$ Thus each jump of the filament at the point of loading due to a discrete rupture event contributes to the time-averaged velocity of the point of loading. These velocities are then, in turn, averaged over 1.5×10^5 realizations of the disordered linker positions along the filament (beyond the broken linker in question). Assuming the motion of the tracer particle in experiments depends solely on the unpeeling of one filament, this quantity reflects the bead's observed velocity; we address the validity of this assumption later in our discussion of the experiments – see Sec. 4.

We plot the probability distributions for $v_\perp/v_0$ in Fig. 7 for tensed (right) and untensed (left) filaments. The most probable peeling velocities as a function of the position of the first unbroken linker x reflect the lattice calculation. The lever-arm effect in the untensed case (left) leads to a high probability of accelerated peeling of the filament even from a disordered array of linkers. Rare "trapping region" configurations of many close linkers produce trapping states that lead to a lower mean velocity of the peeling resulting from a tail of low velocity states in the probability distribution – see the bottom right corner of Fig.7 left. The same feature applies to the tensed case; we see that the highest probability trajectories mimic the predictions of the lattice model. The disordered array of linkers, however, provides new tight-binding regions leading to a significant probability of observing slower peeling dynamics in any realization of the disordered pinning array when compared to the ordered one.

Given the stochastic nature of the peeling dynamics, one expects to observe "ripping events" in which multiple linker rupture in succession over a time short compared to the mean time between such linker ruptures. To look at such ripping events, we calculate the probability of n sequential peeling events occurring over one mean dissociation time $\bar{\tau}$ on a filament bound

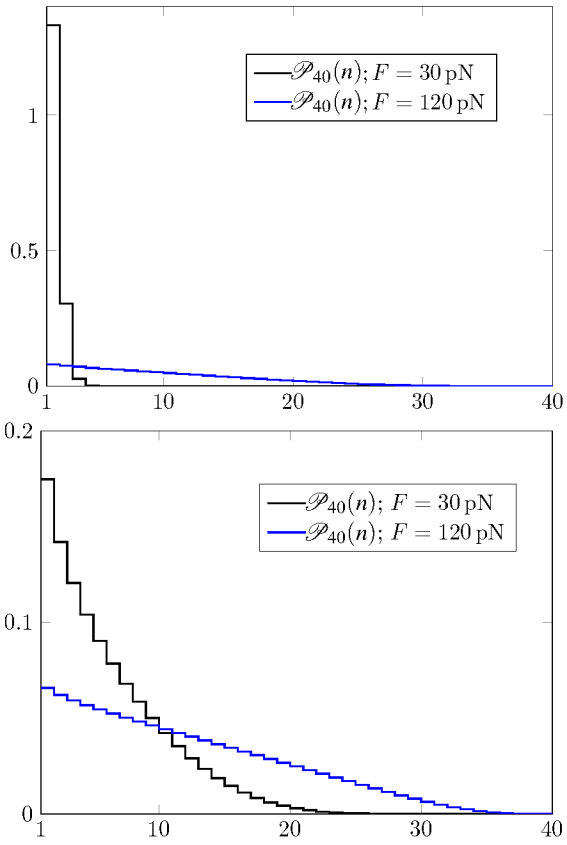

Fig. 8 Distribution of multiple linker rupture events $\mathscr{P}_N(n)$. Top: With tension uncorrelated rupture events are selected from the same Poisson distribution as the loading plateaus. Bottom: Without tension, the lever arm effect accelerates peeling, leading to a higher frequency of fast ruptures or ripping events. $K = 100\,\mathrm{pN}/\mu\mathrm{m}$.

to N cross-linkers, $\mathscr{P}_N(n)$. Specifically, an n-linker rip occurs when a sequence of consecutive linkers rupture with the sum of their waiting times is less than mean time between ruptures: $\tau_i + \ldots + \tau_{i+n-1} \leq \bar{\tau}$. We allow the same τ_i to be part of multiple dissociation types i.e. if $\tau_1 \leq \bar{\tau}$ and $\tau_1 + \tau_2 \leq \bar{\tau}$, then τ_1 contributes to the count of a single dissociation event as well as a sequential 2 cross-linker dissociation event. The high-n tail of this distribution then reflects the expected rarity of such multiple linker rips. These should be observable in experiment as sudden large-scale jumps of the tracer bead under constant load. We discuss this further in Sec 4.

To compute $\mathscr{P}_N(n)$, we created an ensemble of filaments (1.5×10^5 filaments) each with $N = 40$ cross-linkers having a mean spacing, $\bar{\ell}$, of one micron. We looked for ripping events, as defined above, for two different loadings: $F = \{30\,\mathrm{pN}, 120\,\mathrm{pN}\}$ on filaments with and and without applied tension. The results are plotted in Fig. 8.

As expected, the frequency and size of rips both increase with the force for tensed and untensed filaments. The upper set of histograms in Fig. 8 show the frequency of ripping events of various size for tensed filaments. For small forces, the likelihood of n-linker rip decays exponentially with n, consistent with the waiting times between sequential ruptures being uncorrelated and being selected from the same distribution. This can be understood in terms of our mechanics calculation. Once the rip passes down the filament farther than ℓ_κ, the lever-arm effect is suppressed and the loading on first unbroken linker consequently plateaus. Now the Bell model dissociation rate is fixed for all subsequent ruptures. Waiting times for these ruptures are the selected from a fixed Poisson distribution with no correlations between events. This result holds even in the presence of the quenched linker disorder on the filament. It is the bending modulus and the applied tension down the length of the filament that controls the peeling dynamics.

The lower set of histograms in Fig. 8 show the frequency of ripping events of various sizes for untensed filaments. Without tension $\ell_\kappa \to \infty$, the lever arm effect applies for all distances producing an unbounded acceleration of the peeling, which in our currently analysis, appears as a high probability of observing large n ripping events. We observe that the probability of observing large n rips decays more slowly than exponentially for large n (in fact, essentially linearly). Without tension, large ripping events become the norm rather than the exception.

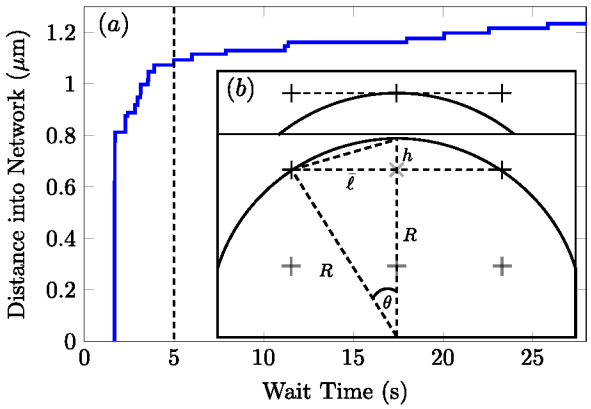

Fig. 9 Representative experimental probe trajectory resolving multiple $\sim$ 10nm scale jumps within the constant velocity regime to the right of the vertical dashed line. (b) Geometric model of the spherical probe of radius R in the semiflexible gel with mesh size $\bar{\ell} = 0.25\mu$m. After linker $\times$ breaks, the probe moves a distance h before contacting the filaments $+$ in the network. For $R \gg \bar{\ell}$, $h \sim 10$nm.

4 Comparison to experiment

There are really two classes of experiments to which our theory should apply. Single filament manipulation of biopolymers such as F-actin or microtubules should provide the most direct test of the theory. One may imagine a single filament being pulled from a regular or disordered array of sticky sites on a substrate (generated perhaps by micro-contact printing techniques[37]). Given that the Bell model parameters are known with reasonable precision for a number of biologically ubiquitous noncovalent bonds (e.g., biotin avidin binding) and that the elastic properties of the semiflexible filaments are well characterized, such single filament measurements provide the most stringent test of the model, one with no fitting parameters.

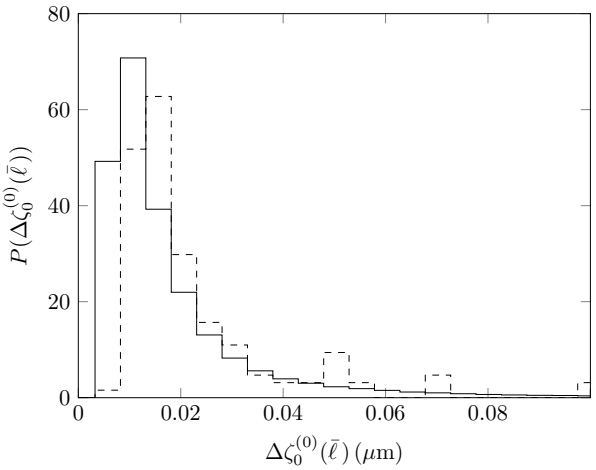

Fig. 10 Dashed Line: Probability distribution of jump sizes for a probe particle under an applied force of 150 pN in a microtubule gel with mesh size$\sim 0.25\,\mu$m. Solid Line: Prediction of jump size distribution for first linker rupture from a disordered linker array with $\bar{\ell} = 0.25\,\mu$m for an untensed filament. $\kappa = 20\,\mathrm{pN}(\mu\mathrm{m})^2$, $K = 100\,\mathrm{pN}/\mu\mathrm{m}$, and $F = 5\,\mathrm{pN}$

As discussed in the introduction, the original inspiration for the theoretical work, however, is found in the many filament experiments in which a large bead (i.e., much bigger than the mesh size of the gel) is moved through the network. This sort of test of the single filament model is necessarily less direct, but we believe that the present single-filament calculation provides at least two key insights into the more complex problem of the gel's dynamics.

First and most generally, the calculations show that the loading of cross-linkers is strongest near the point of force application. In the experiment, there are only a small number (order ten) of filaments in direct contact with the bead. Based on the single filament calculations presented here, we see that the total applied force appears essentially on the first cross-linker away from the bead; the small number of filaments in contact with the bead then divide that load over just a few cross-linkers. This assumption was previously made in order to explain the observed linker-breaking rates as a function of force[28]. The present calculation justifies this assumption.

Our present calculation allows us to address a second and more subtle issue of the observed bead dynamics. Within the apparently constant velocity drift of the bead under load, one observes a spectrum of essentially discontinuous (i.e., more rapid than the data acquisition rate of 60 Hz) jumps of the bead's position, typically on the scale of tens of nanometers. A typical bead trajectory is shown in Fig. 9 by the solid (blue) line. The initial elastic jump and relaxation of the network occur to the left of the dashed vertical line ($t < 5$s); the set of small jumps making up the "constant velocity" drift of the bead occurs for larger times. From these data at larger times, we plot in Fig. 10 the observed distribution of such jumps using a dashed line. Given our predictions for the relative probability of larger ripping events along a single filament, we may ask whether the observed distribution of jumps is consistent with large *n* rips – coordinated ruptures of many linkers along one filament – or simply the result of individual linker ruptures happening independently on different filaments.

To explore the latter hypothesis, we show the expected distribution of bead displacements associated with *single rupture events on a filament* having a Poisson distribution of inter-linker spacing consistent with the experimental gel's mesh size of 0.25μm. This prediction, shown by the solid line in Fig. 10, is consistent with the observed jump distribution once the applied force on that filament is adjusted to 5pN. This suggests that ~ 30 filaments are involved in supporting the full 150pN load on the bead. That estimate is predicted on using a stiff linker spring constant of $100\mathrm{pN}/\mu$m. If this is reduced, one finds the same jump distribution at a larger applied force implying that fewer filaments are engaged. If we were to attempt the to fit the experimental jump frequency data assuming that these jumps are occurring due to multiple sequential rupture evens on one filament, the model would predict larger jumps with too high a frequency to fit the data. Ripping along one filament is inconsistent with these jump frequency data. The picture emerges that the bead's motion is the result of many individual linker ruptures occurring on different filaments in an uncorrelated manner.

Finally, we note that there is a distinct lack of jumps larger than 10nm found in the data. To understand this, consider a simple geometric model of the gel as shown in the inset of Fig. 9. Here the bead is shown as a circular arc while filaments (heading into the page) are shown as crosses $+$, separated by the mesh size ℓ. To calculate the largest expected jump, we assume that when one linker ruptures, that filament no longer is able to support the applied load. The filament with the broken linker is shown as $\times$ in the inset. Upon the rupture, the bead

moves forward a distance h until it impinges upon new filaments in the network. This simple geometric argument leads to an upper limit on bead jumps $h \sim 10$nm, again consistent with the data. These two lines of evidence support the picture that, in the network, bead motion results from the uncorrelated rupture of linkers on one of the few filaments in direct contact with the bead. We conclude that there are no catastrophic ripping events at least for these loads. In other words, there is nothing like crack propagation as a failure mode.

The single filament peeling dynamics in our single filament model are dominated by the interplay between bending and tension, as demonstrated by the role of ℓ_κ in controlling the lever arm effect. Calculations based on the stochastic peeling dynamics of the filament from a regular array of linkers provides a useful and broadly accurate understanding of the more complex problem of peeling a filament from a disordered array of linkers with two caveats: (1) linker disorder generically slows the peeling rate relative to that of the lattice with same mean inter-linker spacing; and (2) there is broad tail of the peeling velocity distribution towards slow peeling rates associated with rare "tight-binding" regions consisting of many closely spaced linkers. The analysis of multi-linker rips and the comparison to experiment points to a picture of dissipative dynamics in the gel associated with the uncorrelated rupture of individual linkers on the various filaments in contact with the probe particle. All rupture events should occur essentially at the nearest cross-link to the probe, i.e., within one mesh size from it. We expect this single-filament work to serve as a foundation for more complex multifilament models of linker rupture and dissipative dynamics in a broad class of semiflexible gels.

5 Acknowledgements

CV would thank D. Kachan, and A. Evans, for their insightful discussions. AJL and CV acknowledge NSF-CMMI-1300514 for partial support. MTV acknowledges NSF-DMR-1410985 and a Career Award at the Scientific Interface from the Burroughs Wellcome Fund for partial support.

A Filament relaxation dynamics

We assume that as cross links are broken, the filament relaxes sufficiently rapidly that it is once again in a static force-balanced state by the time that the next cross linker breaks. Here we briefly justify this separation of time scales. In a fluid with viscosity η, after a cross link breaks, filament segments of length ℓ each relax exponentially to their new mechanical equilibrium configuration on a time scale

$$\tau \sim \frac{\eta \ell^4}{\kappa}, \tag{21}$$

as may be checked simply by dimensional analysis. Shorter segments and stiffer filaments –smaller ℓ and higher κ – relax more quickly. Taking $\ell \sim 0.5\,\mu$m (on the order of a mesh size), the viscosity of water, and a bending modulus consistent with microtubules, we find that $\tau \sim 10^{-5}$ s, significantly shorter than the typical mean time of 1s between linker breaking events observed in experiment – see Fig. 9. In F-actin networks with the same mesh size, one finds the relaxation time to be milliseconds, which is still short compared to mean interval between bond breaking events. We expect this separation of time scales to apply rather widely to bond breaking dynamics in biopolymer networks.

B Effect of different tension on equilibrium equations

We discuss in the text filament statics and peeling dynamics for the cases of zero tension and small, but finite tension, typically chosen to be 1pN or 5pN. Here we discuss in more detail how the value of the tension changes the filament profiles and linker breaking dynamics. For any finite tension, one may rewrite Eq. (3) using rescaled dependent $\bar{\ell}_\kappa^2 = \kappa K^2/\tau^3$ and independent variables $\bar{z} = zK/\tau$ to obtain

$$\left(\bar{\ell}_\kappa^2 \partial_{\bar{z}}^4 - \partial_{\bar{z}}^2\right) \bar{\zeta}(\bar{z}) = \frac{F}{\tau}\delta(\bar{z}) - \sum \delta(\bar{z} - \bar{z}_i)\bar{\zeta}(\bar{z}), \tag{22}$$

with $\bar{\ell}_\kappa^2 = \kappa K^2/\tau^3$. We see that, even upon scaling the applied force by the tension, one does not obtain a universal form for the filament configuration for all tensions. Near the point of force application we expect to see non-universal behavior owing to the residual tension dependence in the scaled bending length $\bar{\ell}_\kappa$, but at long distances from the point of force application, $\bar{z} \gg \bar{\ell}_\kappa$ we expect filament configurations to approach a universal master curve under the appropriate rescaling of the filament vertical displacement $\bar{\zeta}$ and length down the filament $\bar{z}$. In Fig. 4 we show typical filament displacement fields using tensions of 1pN and 5pN.

C Transfer matrix

The transfer matrix necessary for the solution of the mechanics problem discussed in Eq. 8 is given by

$$T(\ell_i) = \begin{pmatrix} 1 & \ell_i & \ell_\kappa^2\left[\cosh \ell_i/\ell_\kappa - 1\right] & \ell_\kappa^3\left[\sinh \ell_i/\ell_\kappa - \ell_i/\ell_\kappa\right] \\ 0 & 1 & \ell_\kappa \sinh \ell_i/\ell_\kappa & \ell_\kappa^2\left[\cosh \ell_i/\ell_\kappa - 1\right] \\ 0 & 0 & \cosh \ell_i/\ell_\kappa & \ell_\kappa \sinh \ell_i/\ell_\kappa \\ -\frac{K}{\kappa} & -\frac{K}{\kappa}\ell_i & \left(\sinh \ell_i/\ell_\kappa - A\left[\cosh \ell_i/\ell_\kappa - 1\right]\right)/\ell_\kappa & \cosh \ell_i/\ell_\kappa - A\left[\sinh \ell_i/\ell_\kappa - \ell_i/\ell_\kappa\right], \end{pmatrix} \tag{23}$$

where $A = (K/\tau)\ell_\kappa$. Thus the transfer matrix depends on the bending length ℓ_κ, the distance between consecutive cross-linkers ℓ_i, and the spring constant K of the linker (though the dimensionless parameter A, defined above). In the limit of

zero tension, $\ell_\kappa \to \infty$ the transfer matrix goes to simpler limiting form:

$$T(\ell_i) = \begin{pmatrix} 1 & \ell_i & \ell_i^2/2! & \ell_i^3/3! \\ 0 & 1 & \ell_i & \ell_i^2/2! \\ 0 & 0 & 1 & \ell_i \\ -\frac{K}{\kappa} & -\ell_i \frac{K}{\kappa} & -\frac{K}{2!\kappa}\ell_i^2 & 1-\frac{K}{3!\kappa}\ell_i^3 \end{pmatrix}$$

In either case, for a fixed array of binding sites, the product of transfer matrices becomes a product of random matrices depending on the quenched random variables ℓ_i. For a regular array of binding sites, this matrix product is easily performed in the diagonal basis. This approach returns us to the discussion of the four eigenvalues of the transfer matrix found in the main text.

D Sequential dissociation approximation

The simplification used in the study of bond breaking dynamics is that we assume the next bond to break is always the first unbroken bond, i.e., the one closest to the point of force application. This sequential dissociation approximation allows for all of the subsequent analysis by determining the breaking trajectories, and may be justified by noting that the first unbroken bond is most strongly loaded. Here we examine the validity of this simplification.

Assuming that the first p cross-linkers have broken, we compute the ratio of the breaking rates of the $p+1$ cross-linker to the breaking rates of the next two bonds: $p+2$ and $p+3$. Using the Bell model, these ratios are $\exp(F_{p+1}-F_{p+2})/F_0$ and $\exp(F_{p+1}-F_{p+3})/F_0$, respectively. As p increases both ratios become progressively larger due to the overall force scale increasing in response to the lever arm effect; this is particularly evident with untensed filaments, where the lever arm effect grows without bound.

For values consistent with microtubules linked by biotin-avidin bonds – $F_0 = 30$pN, see section 3 – we find the breaking rate of the first unbroken linker over the next two to be enhanced by a factor of 2 and 3 respectively. After a few broken bonds, this enhancement factor becomes ~ 10. For larger applied forces (which linearly increase all force scales in our model) and for weaker linkers, i.e., smaller F_0, the dominance of the sequential breaking trajectory becomes even more pronounced. Even for the case of moderate force ($\sim$150pN) and strong bonds considered here, sequential bond breaking is clearly the dominant trajectory after at most a few linker ruptures.

E Master equation for linker rupture

The integral formulation of the probability of the m^{th} bond rupture at time t given by Eq. 14 is a complete solution to the problem of the stochastic dynamics of peeling along any one distribution of linkers; that distribution sets the values of k_i in the integral. The result, however, is more transparent if one takes the time derivative. In that case, due to the sequential breaking approximation, one may write the time derivative of P_m solely in terms of itself and the breakage probability of the last broken cross-linker P_{m-1}:

$$\dot{P}_m(t) = k_m P_{m-1}(t) - k_{m+1} P_m(t), \tag{24}$$

for all but the first cross-linker, i.e., for $m > 0$. The first term represents the increase in breakage probability due to the loss of the $m-1$ cross-linker, making cross-linker m the next to break. The second term represents the breakage of that cross-linker. These equations are supplemented by two more specific to the first

$$\dot{P}_0(t) = -k_1 P_0(t), \tag{25}$$

and last

$$\dot{P}_N(t) = k_N P_{N-1}(t) \tag{26}$$

cross-linker, where clearly only one of these two processes are operative. Finally, one needs the initial conditions $P_m(t=0) = \delta_{m0}$, indicating that no linkers are broken initially. At long times, $P_N(t \to \infty) = 1$; any finite filament eventually becomes completely unbound.

References

1 D. Head, A. Levine and F. MacKintosh, *Phys. Rev. Lett.*, 2003, **91**, 108102.
2 J. Wilhelm and E. Frey, *Phys. Rev. Lett.*, 2003, **91**, 108103.
3 Q. Wen, A. Basu, P. A. Janmey and A. G. Yodh, *Soft Matter*, 2012, **8**, 8039–8049.
4 C. P. Broedersz and F. C. MacKintosh, *Soft Matter*, 2011, **7**, 3186.
5 G. Düring, E. Lerner and M. Wyart, *Soft Matter*, 2012, **9**, 146–154.
6 K. Wang and D. Sun, *Journal of Biomechanics*, 2012, **45**, 1900–1908.
7 C. Semmrich, T. Storz, J. Glaser, R. Merkel, A. R. Bausch and K. Kroy, *Proceedings of the National Academy of Sciences*, 2007, **104**, 20199–20203.
8 O. Lieleg and A. Bausch, *Phys. Rev. Lett.*, 2007, **99**, 158105.
9 H. Kang, Q. Wen, P. A. Janmey, J. X. Tang, E. Conti and F. C. MacKintosh, *J. Phys. Chem. B*, 2009, **113**, 3799–3805.
10 C. P. Broedersz, K. E. Kasza, L. M. Jawerth, S. Münster, D. A. Weitz and F. C. MacKintosh, *Soft Matter*, 2010, **6**, 4120.
11 D. Mizuno, C. Tardin, C. F. Schmidt and F. C. MacKintosh, *Science*, 2007, **315**, 370–373.
12 F. MacKintosh and A. Levine, *Phys. Rev. Lett.*, 2008, **100**, 018104.
13 A. J. Levine and F. C. MacKintosh, *J. Phys. Chem. B*, 2009, **113**, 3820–3830.
14 M. Soares e Silva, M. Depken, B. Stuhrmann, M. Korsten, F. C. MacKintosh and G. H. Koenderink, *Proceedings of the National Academy of Sciences*, 2011, **108**, 9408–9413.

15 T. Thoresen, M. Lenz and M. L. Gardel, *Biophysical Journal*, 2011, **100**, 2698–2705.

16 O. J. N. Bertrand, D. K. Fygenson and O. A. Saleh, *pnas.org*, 2012, 17342–17347.

17 N. Fakhri, A. D. Wessel, C. Willms, M. Pasquali, D. R. Klopfenstein, F. C. MacKintosh and C. F. Schmidt, *Science*, 2014, **344**, 1031–1035.

18 K. Fujiwara, *The Journal of Cell Biology*, 1976, **71**, 848–875.

19 A. R. Bausch and K. Kroy, *Nat Phys*, 2006, **2**, 231–238.

20 M. L. Gardel, I. C. Schneider, Y. Aratyn-Schaus and C. M. Waterman, *Annu. Rev. Cell Dev. Biol.*, 2010, **26**, 315–333.

21 C. Broedersz, C. Storm and F. MacKintosh, *Phys. Rev. Lett.*, 2008, **101**, 118103.

22 P. Chen, *Europhys. Lett.*, 2014, **105**, 38003.

23 B. DiDonna and A. Levine, *Phys. Rev. Lett.*, 2006, **97**, 068104.

24 B. DiDonna and A. Levine, *Phys. Rev. E*, 2007, **75**, 041909.

25 O. Lieleg, M. M. A. E. Claessens and A. R. Bausch, *Soft Matter*, 2010, **6**, 218–225.

26 C. Heussinger, *New J. Phys.*, 2012, **14**, 095029.

27 C. J. Cyron, K. W. Müller, K. M. Schmoller, A. R. Bausch, W. A. Wall and R. F. Bruinsma, *Europhys. Lett.*, 2013, **102**, 38003.

28 Y. Yang, M. Bai, W. S. Klug, A. J. Levine and M. T. Valentine, *Soft Matter*, 2012, **9**, 383.

29 K. W. Müller, R. F. Bruinsma, O. Lieleg, A. R. Bausch, W. A. Wall and A. J. Levine, *Phys. Rev. Lett.*, 2014, **112**, 238102.

30 G. I. Bell, *Science*, 1978, **200**, 618.

31 L. D. Landau and E. M. Lifshitz, *Theory of Elasticity*, Pergamon Press, 1986.

32 Z. Guttenberg, A. R. Bausch, B. Hu, R. Bruinsma, L. Moroder and E. Sackmann, *Langmuir*, 2000, **16**, 8984–8993.

33 P. Benetatos and E. Frey, *Phys. Rev. E*, 2003, **67**, 051108.

34 E. Evans and K. Ritchie, *Biophysical Journal*, 1997, **72**, 1541–1555.

35 J. Rudnick and G. Gaspari, *Elements of the Random Walk: An introduction for Advanced Students and Researchers*, Cambridge University Press, 2004.

36 N. V. Kampen, *Stochastic Processes in Physics and Chemistry*, North-Holland, 2007.

37 L. Lauer, C. Klein and A. Offenhäusser, *Biomaterials*, 2001, **22**, 1925–1932.

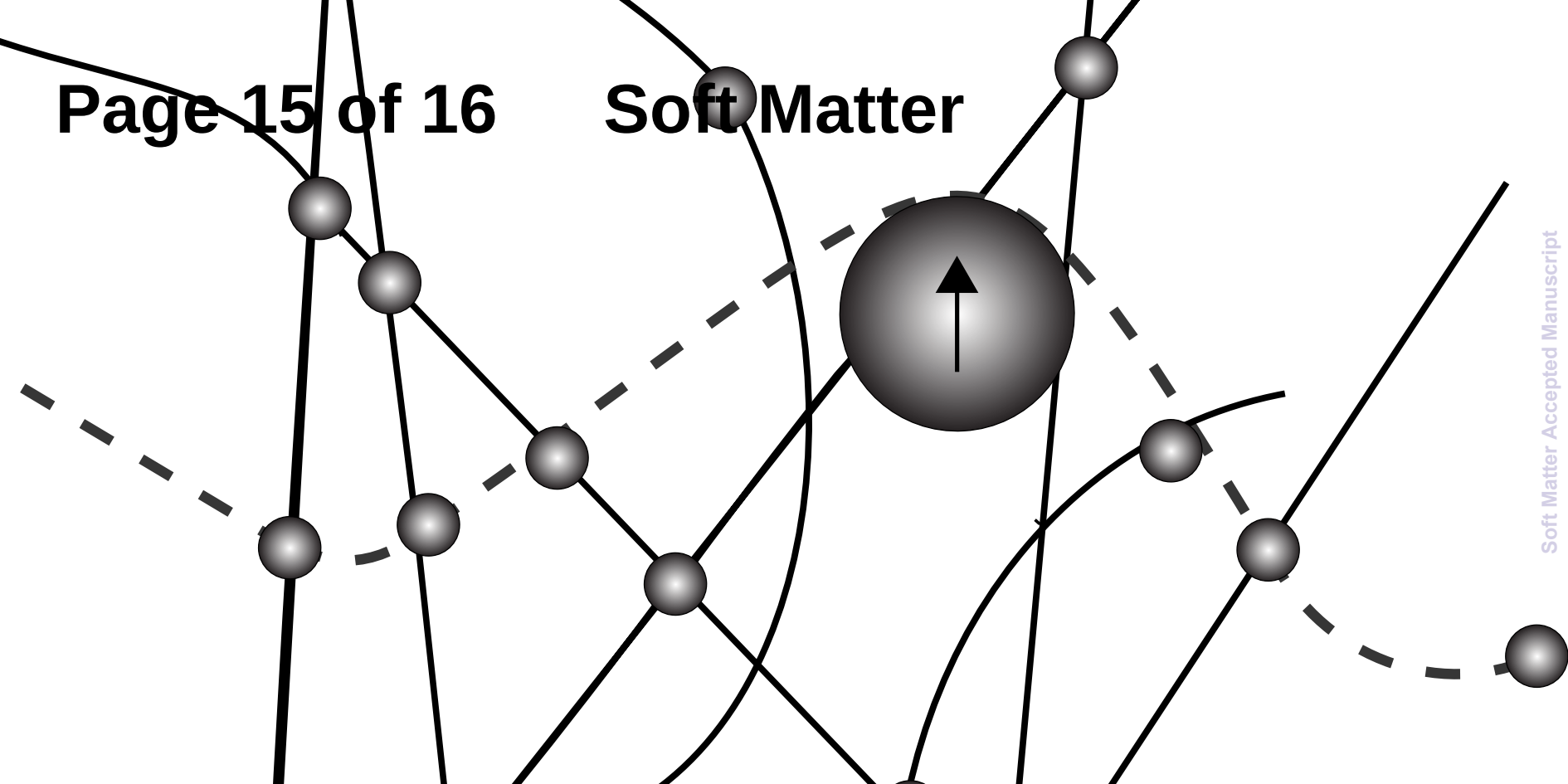

We compute bond-breaking dynamics of a semiflexible filament under loading, and compare to observed driven particle motion in biopolymer networks.